A novel twin reactor for CO_2 photoreduction to mimic artificial photosynthesis

Wei-Hsuan Lee, Chi-Hung Liao, Min-Fei Tsai, Chao-Wei Huang, Jeffrey C.S. Wu*

Department of Chemical Engineering, National Taiwan University, Taipei 10617, Taiwan
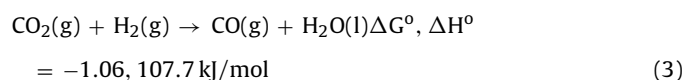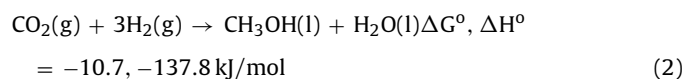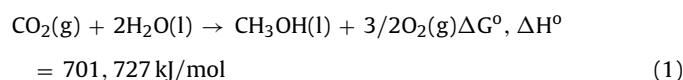
ARTICLE INFO

ABSTRACT

One of the best routes to covert CO_2 into energy and simultaneously reduce atmospheric CO_2 is photosynthesis. In natural photosynthesis, the first step is water splitting in which proton is generated and O_2 is released using solar energy. The second step is the Calvin cycle in which CO_2 is reduced to hydrocarbons. This study demonstrated the photocatalytic hydrogenation of CO_2 by using a novel twin reactor to mimic photosynthesis process in nature. The twin reactor, which divided H_2-generating photocatalyst and O_2-generating photocatalyst in two compartments using a membrane, first achieved separate H_2 and O_2 evolution to prevent the backward reaction to form water under visible light irradiation. The generated hydrogen was then used to perform CO_2 hydrogenation by CO_2 reduction photocatalyst. The advantage is that CO_2 hydrogenation is a spontaneous reaction based on the thermodynamics. The single photocatalyst system using $Pt/CuAlGaO_4$ as both H_2-generating photocatalyst and CO_2 reduction photocatalyst, was compared with the dual photocatalyst system using $Pt/SrTiO_3$:Rh and $Pt/CuAlGaO_4$ as H_2-generating photocatalyst and CO_2 reduction photocatalyst, respectively, under simulated sunlight AM1.5G. The dual photocatalyst system has demonstrated photoreduction quantum efficiency (PQE) of 0.0051%, which is more than doubled the PQE of the single photocatalyst system.

© 2012 Elsevier B.V. All rights reserved.

1. Introduction

The increase of industrial activities in the past few decades has raised the concentration of atmospheric carbon dioxide (CO_2) significantly, causing global warming and drastic change of the world's climate. In view of this, reduction of CO_2 has been studied extensively in recent years and has attracted tremendous of attention from scientists around the world [1]. Recycling of CO_2 via conversion into a high-energy-content fuel, suitable for use in the existing hydrocarbon based energy infrastructure, is an attractive option [2]. Nevertheless, such conversion process is quite challenging due to the fact that CO_2 is a relatively inert and stable compound. Conventionally, methods of CO_2 conversion rely on processes that are energy intense, i.e., reverse water–gas shift (RWGS) reaction [3], meaning that they are not economical and environment-friendly processes. A more clean and sustainable way of converting CO_2 to hydrocarbons is to perform photocatalytic CO_2 reduction, which is carried out under relatively mild conditions with lower energy input [4]. The process is particularly advantageous when the reaction is activated by solar energy, a continuous and readily available power supply. The conversion of CO_2 into hydrocarbons is not necessarily endothermic and equilibrium unfavorable. For instance, the reduction of CO_2 to form methanol

can be represented by 2 possible reactions as shown in Eqs. (1) and (2). The Gibbs free energy and enthalpy of Eq. (1) are positive at 298 K, suggesting that the reaction is equilibrium unfavorable and endothermic. However, the Gibbs free energy and enthalpy of Eq. (2) are negative at 298 K, meaning that the reaction is spontaneous, equilibrium favorable and exothermic [5]. Thus, hydrogenation of CO_2 to produce hydrocarbons is feasible from the thermodynamic viewpoint. Eq. (3) represents the reduction of CO_2 to form CO.

$$CO_2(g) + 2H_2O(l) \rightarrow CH_3OH(l) + 3/2O_2(g) \Delta G^o, \Delta H^o$$
$$= 701, 727 \, kJ/mol \tag{1}$$

$$CO_2(g) + 3H_2(g) \rightarrow CH_3OH(l) + H_2O(l) \Delta G^o, \Delta H^o$$
$$= -10.7, -137.8 \, kJ/mol \tag{2}$$

$$CO_2(g) + H_2(g) \rightarrow CO(g) + H_2O(l) \Delta G^o, \Delta H^o$$
$$= -1.06, 107.7 \, kJ/mol \tag{3}$$

Photocatalytic reduction of CO_2 to hydrocarbons, i.e., formic acid, formaldehyde, methanol, and methane, was first demonstrated by Honda and co-workers in 1979 [6]. The reaction was carried out by suspending both oxide and non-oxide semiconductor particles, including TiO_2, ZnO, CdS, GaP, SiC, and WO_3, in water. Since then, several studies on photocatalytic CO_2 reduction
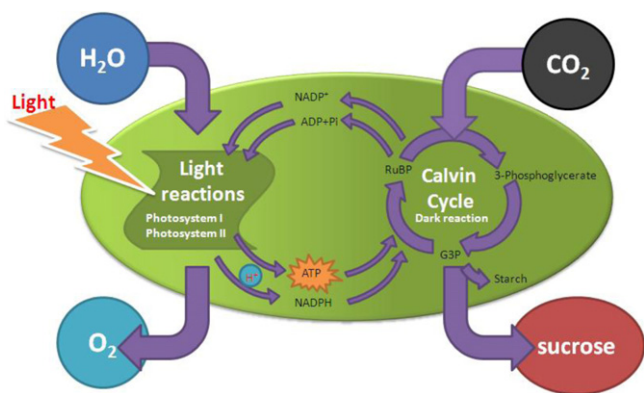
Fig. 1. Concept of photosynthesis.

were reported. Graetzel and co-workers reported the production of methane from a mixture of CO_2 and hydrogen in argon using Ru/RuOx sensitized titania nanoparticles [7]. An initial methane production rate of about $116 \mu L/h$ per $100 mg$ of nanoparticles was obtained, which was believed to be due to the contributions from thermal as well as ultraviolet (UV) light induced effects in the Ru-RuOx/titania system. In 1997, Kohno et al. [8] reported that gaseous carbon dioxide was reduced to carbon monoxide by hydrogen on a ZrO_2 photocatalyst. Among the photocatalysts tested, including TiO_2, ZrO_2, V_2O_5, Nb_2O_5, Ta_2O_5, WO_3 and ZnO, only ZrO_2 was active for this reaction. FT-IR spectroscopy clarified that the surface formate species existed as surface intermediates. Lo et al. [9] confirmed that the photoreduction of carbon dioxide over TiO_2 was enhanced using a gaseous mixture of hydrogen and water vapor to yield methane as a major product, compared with the one using solely hydrogen or water. Guan et al. [10] successfully demonstrated that the hydrogen produced through photocatalytic water splitting could be used for the reduction of carbon dioxide by a hybrid catalyst, in which a Pt-loaded $K_2Ti_6O_{13}$ photocatalyst ($Pt/K_2Ti_6O_{13}$) was combined with an Fe-based catalyst supported on a de-aluminated Y-type zeolite (Fe-Cu-K/DAY) under concentrated sunlight in water. Upon photoirradiation from an Hg lamp around room temperature, the $Pt/K_2Ti_6O_{13}$ photocatalyst promoted the water splitting to produce hydrogen and somewhat reduced carbon dioxide to organic compounds. Even though many studies on CO_2 reduction, particularly CO_2 hydrogenation to form hydrocarbons have been reported, few of them were able to propose a process that can be operated sustainably without the addition of hydrogen continuously during the photoreaction.

In this study, a modified Z-scheme system for water splitting was adopted to carry out CO_2 hydrogenation. The Z-scheme system is comprised of H_2-generating photocatalyst and O_2-generating photocatalyst with the aid of electron transfer mediator (Fe^{2+}/Fe^{3+}) to produce hydrogen and oxygen, respectively in two compartments of a novel twin reactor divided by a membrane [11]. By including CO_2 reduction photocatalyst in the H_2-generating compartment of the twin reactor, the hydrogen generated from water splitting can be used to perform CO_2 hydrogenation directly, so that the addition of hydrogen during the photoreaction can be avoided. This novel process of CO_2 hydrogenation mimics the natural photosynthesis of green plants to convert CO_2 into hydrocarbons. As shown in Fig. 1, there are two steps involved in the chloroplast of green plant during photosynthesis [12]. The first step (left-hand side) is water splitting in which proton is generated and O_2 is released using solar energy. The second step (right-hand side) is a dark reaction called Calvin cycle in which CO_2 taken from atmosphere is reduced to glucose. Proton is carried via NADPH and transferred to the Calvin cycle as hydrogen source, meanwhile

energy is carried by the cycle of ATP and ADP. To prevent the O_2 entering the Calvin cycle is also crucial in the chloroplast because the efficiency will decrease by oxidation.

The combination of CO_2 hydrogenation in the twin reactor proposed here has the following advantages. First, hydrogen and oxygen produced separately in the twin reactor via water splitting will prevent the backward reaction to form water again. Second, hydrogen produced from water splitting can be used directly for CO_2 hydrogenation to achieve sustainable operation without the addition of extra hydrogen during the photoreaction. Last but not least, oxygen from water splitting can be effectively isolated from CO_2 hydrogenation to achieve better efficiency by avoiding the oxidation of hydrocarbon products. In this study, Pt loaded $CuAlGaO_4$ was first used as the H_2-generating and CO_2 reduction photocatalyst. The effect of different Pt loading concentrations on CO_2 hydrogenation efficiency was investigated. Later on, the twin reactor with $Pt/SrTiO_3$:Rh and WO_3 as the H_2-generating photocatalyst and the O_2-generating photocatalyst, respectively was incorporated with $Pt/CuAlGaO_4$ to carry out CO_2 hydrogenation under simulated sunlight.

2. Experimental

2.1. Preparation of photocatalysts

In this study, $Pt/CuAlGaO_4$ was used mainly as the CO_2 reduction photocatalyst. $CuAlGaO_4$ was prepared by the solid-state fusion method [13]. First, powders of CuO, Al_2O_3, and Ga_2O_3 were well mixed in the molar ratio of Cu:Al:Ga = 1:1:1 and pulverized in a mortar to well disperse the mixed powders. The well-mixed powder was calcined at $1150 °C$ for $12 h$ at a rate of $2 °C/min$ in an oven. The calcined powder was then cooled to room temperature and further pulverized to obtain $CuAlGaO_4$. Platinum (Pt) was loaded on $CuAlGaO_4$ by the photo-deposition method as described in the following steps. The H_2PtCl_6 solution of required concentration was mixed with $CuAlGaO_4$ powder to give various wt% of Pt loading (0.5, 1.0, and 1.5 wt%). The well-mixed solution was irradiated by an UV light, which was from the OmniCure series 1500 (USA) with output intensity $5 W/cm^2$, for $1.5 h$ to perform the photo-deposition process. During the process, the solution changed from light-yellow color to colorless, indicating the completion of Pt deposition. The solid product, $Pt/CuAlGaO_4$, was centrifuged and washed by DI water several times to ensure that there was no residual Cl^- on the material. Finally, the washed material was dried at $80 °C$ in an oven to give $Pt/CuAlGaO_4$ powder.

$Pt/SrTiO_3$:Rh was used as the H_2-generating photocatalyst. It was prepared by the sol–gel method similar to the one reported by Wang et al. [14]. First, citric acid solution (3.1521 g of citric acid in 50 mL DI water) was mixed with $RhCl_3$ solution (0.0209 g of $RhCl_3$ in 20 mL DI water). $Sr(NO)_3$ powder was added into the above mixture in the molar ratio of citric acid:$Sr(NO)_3$ = 1:1.5 and well mixed. Few drops of glycol were then added into the mixture to stabilize the reaction while the pH of the mixture was maintained at 1.5. At this time, 4.2387 g of $Ti(OBu)_4$ was added into the mixture to start the sol–gel reaction. The mixture was allowed to react inside a dry glove box for $25 h$ to obtain the sol. The sol was then dried in an oven at $80 °C$ and calcined at $1000 °C$ for $10 h$ at a rate of $10 °C/min$ under air condition. Finally, the calcined powder was then cooled to room temperature and further pulverized to obtain $SrTiO_3$:Rh. Platinum (Pt) was loaded on $SrTiO_3$:Rh by the photo-deposition method as described previously for the preparation of $Pt/CuAlGaO_4$ where the H_2PtCl_6 solution of known concentration was mixed with $SrTiO_3$:Rh powder to give 0.8 wt% of Pt loading. Commercial WO_3 (99.9%) supplied from Hayashi Pure Chemical was used as the O_2-generating photocatalyst and pulverized prior to application.

Table 1
EDS analysis of various photocatalysts.

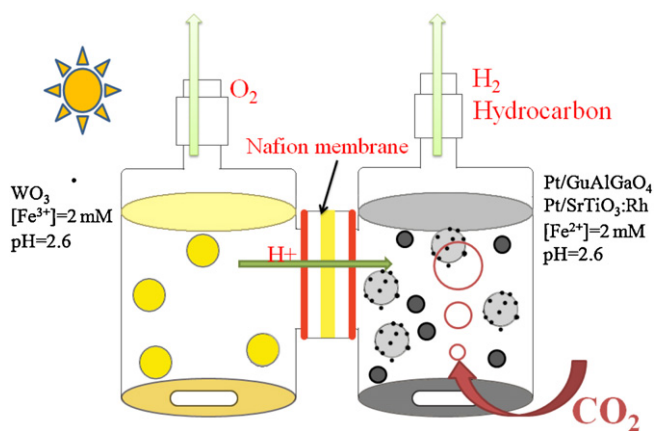| Sample	Atomic (%)				
CuAlGaO$_4$	Cu 12.34	Al 10.94	Ga 16.37	O 60.36	
Pt(1.0 wt%)/CuAlGaO$_4$	Cu 11.58	Al 14.17	Ga 11.19	O 62.99	Pt 0.07
Pt(0.8 wt%)/SrTiO$_3$:Rh	Sr 16.71	Ti 17.03	O 66.26	Rh BDL	Pt BDL
WO$_3$	W 23.02	O 76.98			

BDL: below detection limit.

Fig. 2. Schematic diagram of the novel twin reactor system.

2.2. Characterization of photocatalysts

For photocatalyst characterization, the crystallinity of photo-catalysts was obtained with a Bruker-D8-ADVANCE X-ray diffrac-tometer (XRD) in the diffraction angle (2θ) between 20 and 80°, using Cu Kα radiation as the source. The X-ray (wavelength $\lambda = 1.5405$ Å) tube equipped with copper target was operated at 40 kV and 30 mA. The scanning rate was 3°/min. The crystal size was calculated using Scherrer's equation. The UV–vis absorption spectra of photocatalysts were measured by a diffusive reflectance UV–vis spectrometer (Varian Cary-100) in the wavelength range between 200 and 800 nm at a scanning rate of 120 nm/min. Field emission scanning electron micrograph (FE-SEM) was car-ried out on a Hitachi model S-800. The photocatalyst was sputtered with a thin film of Pt to prevent surface charging and to pro-tect the surface material from thermal damage by the electron beam. Specific surface area of photocatalyst was identified by Brumauer–Emmett–Teller (BET) method based on the Langmuir isotherm absorption. Before the BET measurement by Micromer-itics ASAP2020/C5-05, the photocatalysts were heated at 300 °C to remove water vapor and then nitrogen was introduced as the absorbate. For surface analysis, X-ray photoelectron spectroscopy (XPS) was conducted to identify the composition of photocatalysts by using Thermo Scientific, Theta probe X-ray with Mg target as the source to generate energy of 1253.6 eV. The passing energy was 200 eV with 30 scanning cycles.

2.3. CO$_2$ photoreduction apparatus and reactions

For the water splitting combined CO$_2$ photoreduction reaction, two sets of experiment were performed. In the first set, 0.30 g of Pt/CuAlGaO$_4$ in 2 mM FeCl$_2$ solution and 0.30 g of WO$_3$ in 2 mM FeCl$_3$ solution were placed respectively in the H$_2$-generating com-partment and the O$_2$-generating compartment of a connected twin reactor separated by a circular Nafion membrane as shown in Fig. 2. The volume of solution in each compartment was 225 mL and the pH of solution was adjusted to 2.6 by adding sulfuric acid to prevent precipitation of the iron solution [15]. During the photoreaction, the solution in each compartment was stirred and irradiated with a 300 W xenon (Xe) lamp placed at equal-distance from both compartments so that both solutions have received the same amount of light intensity (mostly visible light), which was around 270 mW/cm^2. The purpose of performing the first set of experiment is to determine the optimum loading of Pt for Pt/CuAlGaO$_4$ which acted as both H$_2$-generation and CO$_2$ reduc-tion photocatalysts. In the second set of experiment, the conditions were the same as above except that 0.15 g of Pt/CuAlGaO$_4$ and

0.15 g of Pt/SrTiO$_3$:Rh, acting as CO$_2$ reduction and H$_2$-generating photocatalyst respectively, were placed in the H$_2$-generating com-partment. In addition, the light source used was a 300 W xenon lamp equipped with an AM1.5 G filter to give a light intensity of approximately 90 mW/cm^2. Before light irradiation, ultra-pure Ar gas was introduced to purge the solution in the O$_2$-generating com-partment of the reactor system for 12 h to remove any dissolved gas while ultra-pure CO$_2$ gas was introduced to purge the solu-tion in the H$_2$-generating compartment. The produced oxygen and hydrogen gases in each compartment of the reactor system were collected separately every 2 h by an on-line sampling loop (1 mL) and further analyzed by the gas chromatography (China GC 2000) system equipped with thermal conductivity detector (TCD) and 3.5 m long molecular sieve 5A packed column to determine the con-centration. Ultra-pure Ar (99.9995 v%) was used as the carrier gas for GC. Moreover, the solution in the H$_2$-generating compartment of the reactor system was sampled every 2 h and analyzed by another gas chromatography (China GC 2000) system equipped with flame ionization detector (FID) and 2 m long Porapak QS packed column to determine the concentration of organic products or byprod-ucts. A liquid sample of 1–10 μL was taken from the reactor then injected in GC after filtering catalyst. Analysis results indicated that methanol was the dominant hydrocarbon. A calibration curve of methanol was established, and used to calculate the concentra-tion from the GC integration area of FID peak. The concentration of methanol was converted to the total amount in the reactor based on the volume ratio of reactor and injected sample. To further increase the detection limit of CO, the GC was also connected to a methanizer which selectively transforms CO to CH$_4$ with H$_2$ at 360 °C using a Ni catalyst. The injected sample was separated by the GC column first, and then carried by helium into the methanizer. After the CO signal appeared on the GC spectrum, the sample stream was switched to another exit to avoid high concentration CO$_2$ being carried into the methanizer. Then the sample stream was switched back to analyze other products after purging out CO$_2$. Thus CO can be quantitatively measured indirectly by the FID in the GC.

3. Results and discussion

Fig. 3 shows the SEM images of (a) CuGaAlO$_4$, (b) Pt(1.0 wt%)/CuGaAlO$_4$, (c) WO$_3$ and (d) Pt(0.8 wt%)/SrTiO$_3$:Rh with 10 K magnification. It is apparent that CuGaAlO$_4$ has cube-like shape and smooth surfaces, while WO$_3$ has sphere-like shape and smaller particle size comparing with CuGaAlO$_4$. In contrary, SrTiO$_3$:Rh has irregular shape compared with other photocatalysts. It is also noted that loading of Pt on CuGaAlO$_4$ or SrTiO$_3$:Rh could not be observed and did not change the shape and morphology of the photocatalyst (image of SrTiO$_3$:Rh is not shown) after the Pt photo-deposition. To further investigate the chemical composition of the prepared photocatalysts, EDS analysis was performed and the results are shown in Table 1. For CuGaAlO$_4$ based photocata-lysts, the ratio of Cu:Ga:Al:O is roughly near the stoichiometric
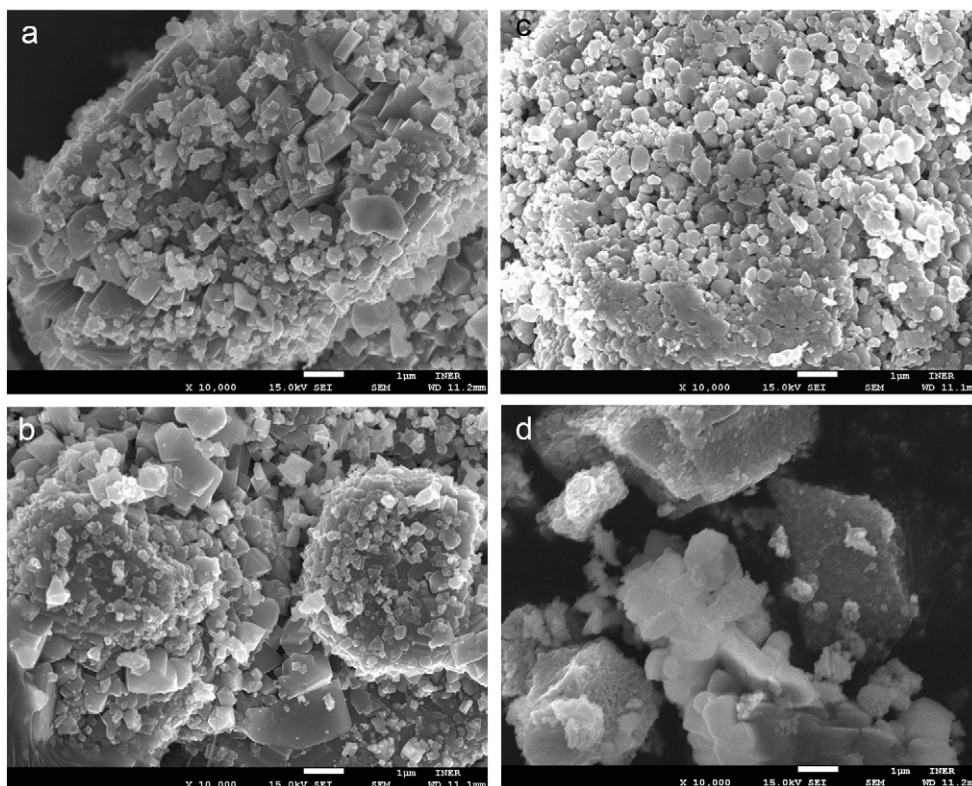
Fig. 3. SEM images of (a) CuGaAlO$_4$, (b) Pt(1.0 wt%)/CuGaAlO$_4$, (c) WO$_3$, and (d) Pt(0.8 wt%)/SrTiO$_3$:Rh.

ratio, confirming the presence of CuGaAlO$_4$. Moreover, signal of Pt was observed for Pt(1.0 wt%)/CuGaAlO$_4$, suggesting that Pt was successfully loaded on the photocatalyst. For WO$_3$, the ratio of W to O detected is consistent with its stoichiometric ratio, which is 1 to 3. As for Pt(0.8 wt%)/SrTiO$_3$:Rh, the ratio of Sr:Ti:O is approximately to the stoichiometric ratio 1:1:3, suggesting the presence of SrTiO$_3$. However, photo-deposited Pt and doped Rh were not detectable by EDS due to very small amounts. Another evidence for the existence of Pt particles on the surface of Pt(1.0 wt%)/CuGaAlO$_4$ and Pt(0.8 wt%)/SrTiO$_3$:Rh is revealed from the XPS analysis. The XPS spectra of Pt(1.0 wt%)/CuGaAlO$_4$ and Pt(0.8 wt%)/SrTiO$_3$:Rh shown in Fig. 4 elucidate the chemical status of Pt on the surface of CuGaAlO$_4$ and SrTiO$_3$:Rh. Two binding-energy peaks are observed in the XPS spectra of Pt for both photocatalysts. The peaks at

74.5 and 78.3 eV, respectively corresponds to 4f$_{7/2}$ and 4f$_{5/2}$ of Pt oxide, implying the presence of Pt. The formation of Pt oxide might be attributed to the low UV light intensity used during the photo-deposition process, leading to insufficient reduction efficiency for Pt. The specific surface areas of photocatalysts, CuGaAlO$_4$, Pt(1.0 wt%)/CuGaAlO$_4$, Pt(0.8 wt%)/SrTiO$_3$:Rh and WO$_3$ are 0.53, 1.99, 3.83, and 4.01 m^2/g, respectively.

To investigate the crystallinity of the prepared photocatalysts, X-ray diffraction spectrometry was conducted. Fig. 5 shows the XRD patterns of CuGaAlO$_4$, Pt(1.0 wt%)/CuGaAlO$_4$, Pt(0.8 wt%)/SrTiO$_3$:Rh and WO$_3$. For CuGaAlO$_4$, its XRD pattern is identical to that reported in the literature [13]. The loading of Pt did not change the XRD pattern of CuGaAlO$_4$ because only small amount of Pt was present. The crystallinity of Pt(0.8 wt%)/SrTiO$_3$:Rh
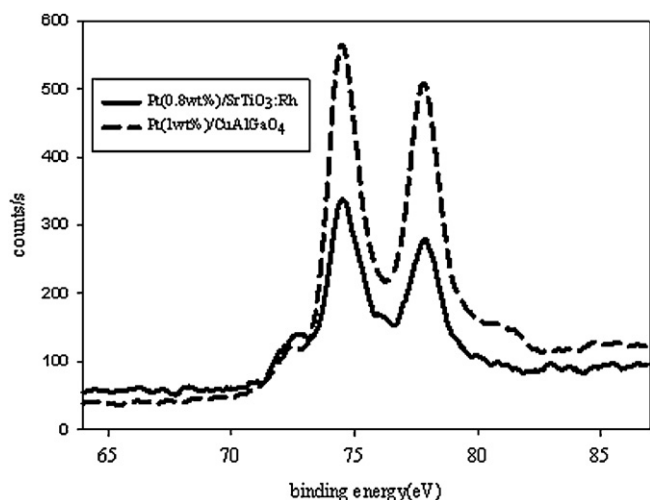
Fig. 4. Pt 4f$_{7/2}$ XPS spectra of Pt(1.0 wt%)/CuAlGaO$_4$ and Pt(0.8 wt%)/SrTiO$_3$:Rh.
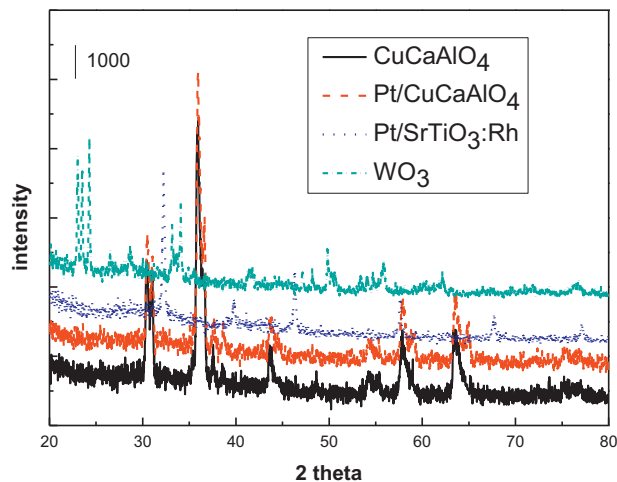
Fig. 5. XRD patterns of CuGaAlO$_4$, Pt(1.0 wt%)/CuGaAlO$_4$, Pt(0.8 wt%)/SrTiO$_3$:Rh and WO$_3$.
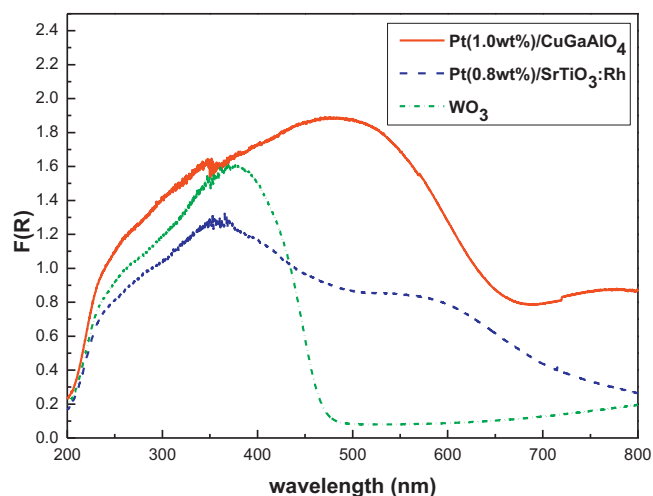
Fig. 6. UV–vis absorption spectra of Pt(1.0 wt%)/CuGaAlO$_4$, Pt(0.8 wt%)/SrTiO$_3$:Rh, and WO$_3$.

Fig. 7. Amount of (a) hydrogen, (b) methanol, and (c) CO produced in the H$_2$-generating compartment of the twin reactor for different Pt/CuGaAlO$_4$ photocatalysts.

is consistent with that of SrTiO$_3$ based on the JCPDS-Power Diffraction File. The diffraction peaks of Rh and Pt are absent mainly due to the little amount of Rh and Pt used as well. Based on Scherrer's equation, the crystal size of Pt(1.0 wt%)/CuGaAlO$_4$ and Pt(0.8 wt%)/SrTiO$_3$:Rh is estimated to be 21.80 and 41.28 nm, respectively. As for the purchased WO$_3$ photocatalyst, its diffraction peaks are consistent with that of orthorhombic WO$_3$ from JCPDS-Power Diffraction File. The calculated crystal size of WO$_3$ is 155 nm. The UV–vis absorption spectra of Pt(1.0 wt%)/CuGaAlO$_4$, Pt(0.8 wt%)/SrTiO$_3$:Rh, and WO$_3$ are presented in Fig. 6. An absorption band at around 450–650 nm is observed for Pt/SrTiO$_3$:Rh mainly due to the doping of Rh atoms, which suggests that Pt/SrTiO$_3$:Rh is a visible-light photocatalyst. This result is consistent with the one reported by Kudo and co-workers [16], which indicated that doping of Rh in SrTiO$_3$ may provide extra donor level for SrTiO$_3$, resulting in the shift of its conduction band to more negative potential. Apparently, the O$_2$-generating photocatalyst (commercial WO$_3$) used in this study is a visible-light-response photocatalyst as well since its absorption edge extended to visible-light region at around 480 nm. As for Pt(1.0 wt%)/CuGaAlO$_4$, absorption of light from 250 nm up to 670 nm is observed, indicating that Pt(1.0 wt%)/CuGaAlO$_4$ is also a visible light-active photocatalyst. Based on the UV–vis absorption spectra, the band gap of Pt(1.0 wt%)/CuGaAlO$_4$, Pt(0.8 wt%)/SrTiO$_3$:Rh, and WO$_3$ is calculated to be 1.72, 2.31, and 2.58 eV, respectively.

The activity of prepared photocatalyst toward oxygen, hydrogen and hydrocarbon generation is demonstrated by conducting the water splitting combined CO$_2$ photoreduction in the twin reactor under visible-light irradiation. Fig. 7(a) shows the hydrogen produced per gram of photocatalyst in the H$_2$-generating compartment of the twin reactor for different Pt/CuGaAlO$_4$ photocatalysts with various Pt loadings. After 6 h of reaction, the total amount of hydrogen produced seems to increase with the amount of Pt loaded on the CuGaAlO$_4$ photocatalyst up to Pt loading of 1.0%. This implies that loading of Pt can improve the activity of photocatalyst by trapping photogenerated electrons to minimize electron-hole recombination [17]. However, as Pt loading reaches 1.5%, the loaded Pt particles may aggregate on the surface of the CuGaAlO$_4$, leading to reduced surface area of active sites on the photocatalyst and lower photoactivity. The Pt/CuGaAlO$_4$ photocatalyst used in this set of experiment can act not only as H$_2$-generating photocatalyst, but also as CO$_2$ reduction photocatalyst. Fig. 7(b) illustrates the methanol produced per gram of photocatalyst as a result of CO$_2$ reduction in the H$_2$-generating compartment of the twin reactor
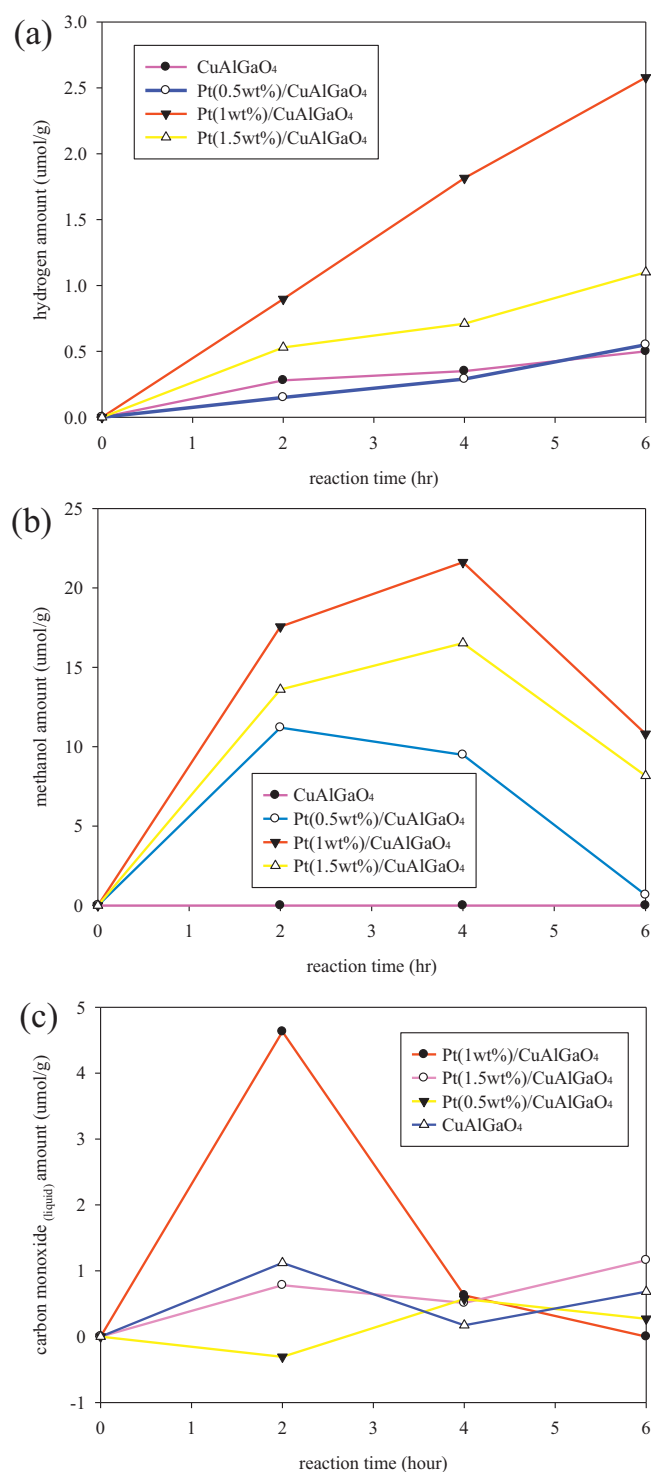
for different Pt/CuGaAlO$_4$ photocatalysts. Apparently, the trend of methanol produced is similar to that of hydrogen generated, i.e., the amount of methanol produced is directly proportional to the amount of Pt loaded on CuGaAlO$_4$, with the exception of Pt loading of 1.5%. The result confirms that Pt/CuGaAlO$_4$ indeed can be a H$_2$-generating photocatalyst and a CO$_2$ reduction photocatalyst. Moreover, the hydrogen generated via water splitting can facilitate CO$_2$ photoreduction to form methanol. It is noteworthy that the

rate of methanol production starts to decrease after 2 h of photoreaction. We had detected trace amount of acetaldehyde in some experiments. Thus one possibility is that methanol converts to 2-carbon compounds by the secondary reaction although we did not measured them quantitatively. The other reason may be attributed the oxidization by the photogenerated holes on Pt/CuGaAlO$_4$, while photogenerated electrons are used to reduce protons to form hydrogen. However, the holes on Pt/CuGaAlO$_4$ (or Pt/SrTiO3:Rh) should have much higher possibility to be quickly neutralized by the Fe^{2+} than to oxidize methanol because of high concentration of Fe^{2+} (2 mM) in the H$_2$-generating compartment. Fig. 7(c) shows the amount of CO produced, an intermediate of CO$_2$ photoreduction, in the H$_2$-generating compartment of the twin reactor for different Pt/CuGaAlO$_4$ photocatalysts. In general, the yield of CO increases initially, and then decreases as the photoreaction goes on. This is because CO is an intermediate species. As the reaction proceeds, CO produced will be further reduced to methanol. Again, Pt(1.0 wt%)/CuGaAlO$_4$ exhibits the most drastic change in CO concentration, implying that Pt(1.0 wt%)/CuGaAlO$_4$ is the most active photocatalyst among those tested. Based on the results above, it is concluded that the optimal loading of Pt on CuGaAlO$_4$ in this study is 1.0% and hydrogen has a positive effect on methanol yield.

To further improve the efficiency of CO$_2$ photoreduction, Pt(1.0 wt%)/CuGaAlO$_4$, as the optimal CO$_2$ reduction photocatalyst, was combined with a highly efficient H$_2$-generating photocatalyst, Pt(0.8 wt%)/SrTiO$_3$:Rh [15], and placed in the H$_2$-generating compartment of the twin reactor to carry out the same photoreaction again. This time, the light source used was a 300 W Xe lamp equipped with AM1.5 G filter to simulate sunlight. The yields of oxygen (in O$_2$-generating compartment), hydrogen (in H$_2$-generating compartment), methanol (in H$_2$-generating compartment) and CO (in H$_2$-generating compartment) are shown in Fig. 8(a) and (b). It is interesting to note that the yield of hydrogen is lower than that of oxygen, different from the result of typical water splitting. This is due to the fact that part of the hydrogen produced was consumed by the CO$_2$ reduction reaction. Furthermore, the trend of methanol production is inversely correlated with the trend of CO production as expected, meaning that CO as an intermediate was oxidized and consumed to form methanol. To compare the photoreduction efficiency of single photocatalyst system (Pt/CuGaAlO$_4$ only as the reduction photocatalyst) with that of dual photocatalyst system (Pt/CuGaAlO$_4$ and Pt/SrTiO$_3$:Rh as the reduction photocatalyst), a term called photoreduction quantum efficiency (PQE) is defined as shown in Eq. (4):

$$\frac{n_e \times \text{Product formation rate (nmole/h)}}{\text{Incident photon rate (nmole/h)}} \times 100\% = \text{PQE} \qquad (4)$$

where n_e is the number of moles of electrons needed to reduce 1 mole of reactant to 1 mole of product. The rate of incident photon can be calculated by Eq. (5):

$$\frac{I_{\text{int}} (\text{W/m}^2) \times A_{\text{proj}} (m^2)}{hc/\lambda (\text{J/\# of photon})} = \text{Incident photon rate} \qquad (5)$$

where I_{int} is the incident light intensity, A_{proj} is the area of light irradiation projected on the reactor (3.89×10^{-3} m^2), h is the Plank constant, c is the speed of light and λ is the wavelength of light (assume 555 nm, the wavelength used by the light meter for intensity measurement). The results of product formation rates, incident photon rates and total PQEs for single photocatalyst system and dual photocatalyst system are summarized in Table 2. As expected, the incorporation of a H$_2$-generating photocatalyst, Pt(0.8 wt%)/SrTiO$_3$:Rh, significantly improves the efficiency of the photoreduction reaction. The PQE has been increased by more than 2-fold from 0.0019% to 0.0051%. The improvement is mainly due to the fact that Pt(0.8 wt%)/SrTiO$_3$:Rh is a better H$_2$-generating photocatalyst than Pt(1.0 wt%)/CuGaAlO$_4$ and the enhanced H$_2$ yield
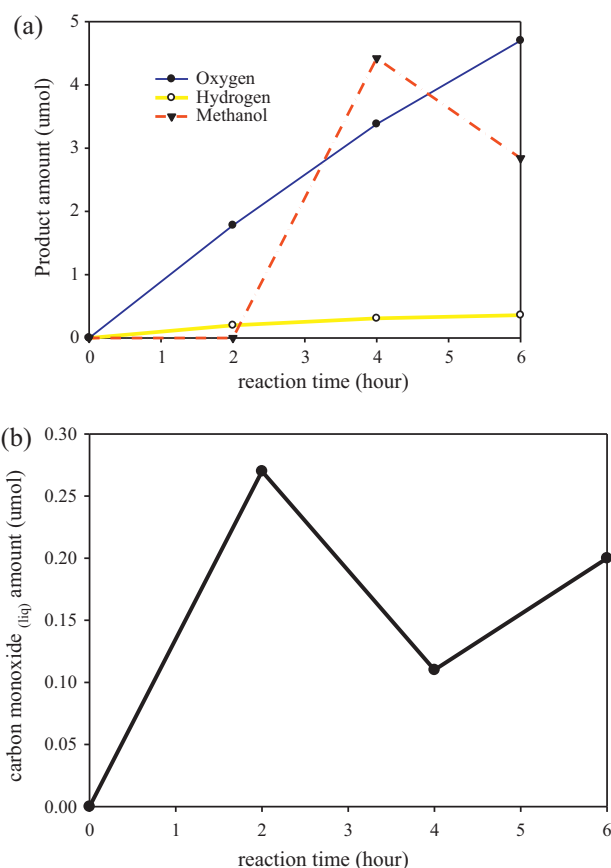

Fig. 8. Amount of (a) oxygen, hydrogen, methanol, and (b) CO produced during the photoreaction using dual photocatalyst system.

further promotes the efficiency of CO$_2$ photoreduction. To further prove that hydrogen produced was utilized to carry out the CO$_2$ reduction reaction, molar ratio of the generated hydrogen to oxygen was calculated by Eq. (6):

$$\frac{n\text{H}_2 + 3n_{\text{CH}_3\text{OH}} + n_{\text{CO}}}{n_{\text{O}_2}} = \text{Molar ratio of H}_2 \text{ to O}_2 \qquad (6)$$

where $n\text{H}_2$ is the number of moles of hydrogen produced, $n_{\text{CH}_3\text{OH}}$ is the number of methanol produced and n_{CO} is the number of oxygen produced. The above equation assumes that hydrogenation of CO$_2$ carried out in this study is most likely to form methanol and carbon monoxide according to Eqs. (2) and (3), which is reasonable due to their negative Gibbs free energy values. In fact, methanol and carbon monoxide are the two major species detected in this study.

Table 2
PQE of single photocatalyst system and dual photocatalyst system.

Parameters	Results	
	Single photocatalyst system	Dual photocatalyst system
Incident photon rate	2.93×10^{19} (# of photon/s)	9.78×10^{18} (# of photon/s)
H$_2$ formation rate	124.7 nmole/h	60.0 nmole/h
Methanol formation rate	522.0 nmole/h	473.3 nmole/h
CO formation rate	7.7 nmole/h	13.3 nmole/h
n_e for H$_2$	2	2
n_e for methanol	6	6
n_e for CO	2	2
Total PQE	0.0019%	0.0051%
H$_2$-to-O$_2$ molar ratio	2.05	1.89

Eq. (6) also assumes that 1 mole of methanol produced will consume 3 moles of hydrogen, whereas 1 mole of carbon monoxide produced will only consume 1 mole of hydrogen. The calculated hydrogen-to-oxygen molar ratio is 2.05 and 1.89 for single and dual photocatalyst system respectively (Table 2), nearly matching with the ideal hydrogen-to-oxygen ratio in water which is 2. This implies that most of the hydrogen produced during the water splitting indeed was used by the CO_2 reduction reaction to form methanol and carbon monoxide.

4. Conclusion

In this study, a novel twin reactor was used to mimic natural photosynthesis, which is the best way to convert CO_2 into energy and simultaneously reduce the global CO_2 level. The advantage of twin reactor is that O_2 is isolated from the reduction reaction so the backward oxidation of H_2 and hydrocarbons can be prevented. First part of this study was to evaluate the activity of various $Pt/CuGaAlO_4$ photocatalysts under visible light. It was found that Pt loading of 1.0 wt% gave the highest photoactivity in terms of hydrogen and methanol production. In the second part of this study, $Pt(1.0 wt\%)/CuGaAlO_4$ was selected and combined with a highly efficient H_2-generating photocatalyst, $Pt(0.8 wt\%)/SrTiO_3$:Rh to perform the same photoreaction again under AM1.5G. The incorporation of a H_2-generating photocatalyst significantly improved the efficiency of the photoreduction reaction. The PQE has been increased by more than 2-fold from 0.0019% to 0.0051%. The improvement is mainly due to the fact that $Pt(0.8 wt\%)/SrTiO_3$:Rh is a better H_2-generating photocatalyst than $Pt(1.0 wt\%)/CuGaAlO_4$ and the enhanced H_2 yield further promotes the efficiency of CO_2 photoreduction. Currently the overall quantum efficiency of CO_2 photoreduction is still low compared with nature photosynthesis. However, the twin-reactor system is not optimized to achieve a maximum efficiency, e.g., the best combination of H_2-generation and CO_2 reduction catalysts. We expect the PQE of twin reactor can be significantly improved by further study.

Acknowledgement

References

[1] V.P. Indrakanti, J.D. Kubicki, H.H. Schobert, Energy and Environmental Science 2 (2009) 745–758.
[2] O.K. Varghese, M. Paulose, T.J. LaTempa, C.A. Grimes, Nano Letters 9 (2009) 731–737.
[3] C.S. Chen, W.H. Cheng, Catalysis Letters 83 (2002) 121–126.
[4] J.C.S. Wu, H.M. Lin, International Journal of Photoenergy 7 (2005) 115–119.
[5] Xu, J.A. Moulijn, Energy and Fuels 10 (1996) 305–325.
[6] T. Inoue, A. Fujishima, S. Konishi, K. Honda, Nature 277 (1979) 637–638.
[7] K.R. Thampi, J. Kiwi, M. Gratzel, Nature 327 (1987) 506–508.
[8] Y. Kohno, T. Tanaka, T. Funabiki, S. Yoshida, Chemical Communications (1997) 841–842.
[9] C.-C. Lo, C.-H. Hung, C.-S. Yuan, J.-F. Wu, Solar Energy Materials and Solar Cells 91 (2007) 1765–1774.
[10] G.Q. Guan, T. Kida, A. Yoshida, Applied Catalysis B: Environmental 41 (2003) 387–396.
[11] C.C. Lo, C.W. Huang, C.H. Liao, J.C.S. Wu, International Journal of Hydrogen Energy 35 (2010) 1523–1529.
[12] J.N. Armor, Catalysis Letters 114 (2007) 115–121.
[13] S.K. Biswas, J.O. Baeg, B.B. Kale, R.K. Yadav, S.J. Moon, K.J. Kong, W.W. So, Catalysis Communications 12 (2011) 651–654.
[14] X.W. Wang, Z.Y. Zhang, S.X. Zhou, Materials Science and Engineering B-Solid State Materials for Advanced Technology 86 (2001) 29–33.
[15] S.C. Yu, C.W. Huang, C.H. Liao, J.C.S. Wu, S.T. Chang, K.H. Chen, Journal of Membrane Science 382 (2011) 291–299.
[16] R. Konta, T. Ishii, H. Kato, A. Kudo, Journal of Physical Chemistry B 108 (2004) 8992–8995.
[17] G.R. Bamwenda, S. Tsubota, T. Nakamura, M. Haruta, Journal of Photochemistry and Photobiology A: Chemistry 89 (1995) 177–189.